Author Manuscript
Accepted for publication in a peer-reviewed journal

NIST National Institute of Standards and Technology • U.S. Department of Commerce

Published in final edited form as:
Appl Phys Lett. 2016 ; 109(8): . doi:10.1063/1.4961881.

Influence of internal geometry on magnetization reversal in asymmetric permalloy rings

D. B. Gopman[1,*], **Y. P. Kabanov**[1,2], **J. Cui**[3], **C. S. Lynch**[3], and **R. D. Shull**[1]

[1]Materials Science and Engineering Division, National Institute of Standards and Technology, Gaithersburg, MD 20899, USA

[2]Institute for Solid State Physics, Russian Academy of Sciences, Chernogolovka, Moscow Region 142432, Russia

[3]Department of Mechanical and Aerospace Engineering, University of California, Los Angeles, 90095 CA, USA

Abstract

We report the magnetization reversal behavior of microstructured $Ni_{80}Fe_{20}$ rings using magneto-optic indicator film imaging and magnetometry. While the reversal behavior of rings with a symmetric (circular) interior hole agrees with micromagnetic simulations of an onion → vortex → onion transition, we experimentally demonstrate that rings possessing an elliptical hole with an aspect ratio of 2 exhibit complex reversal behavior comprising incoherent domain propagation in the rings. Magneto optic images reveal metastable magnetic configurations that illustrate this incoherent behavior. These results have important implications for understanding the reversal behavior of asymmetric ferromagnetic rings.

Controlling the magnetization dynamics in thin ferromagnetic rings generates broad interest due to their potential in high density storage and in micro– and nano–electromechanical motors.[1–4] For applications requiring the zero–flux–closure vortex state, symmetric rings with a concentric hole have been shown to be unsuitable, as the metastable “onion” state dominates the reversal dynamics under uniform applied external fields.[5,6] Consequently, recent studies have examined the possibility of selecting the preferred magnetization state by breaking the symmetry of the rings. Rings that possess a thickness gradient across a reflection axis have shown an enhanced probability of a vortex configuration.[7] Micromagnetic simulations and experimental realization have also shown that rings with an offset hole (i.e., non–concentric) are also able to generate the vortex state with higher probability than in concentric rings.[7–9] Such asymmetric rings with non–concentric holes also show enhanced domain wall propagation when compared to their concentric counterparts.[10,11]

In this letter, we explore an additional mode for introducing asymmetry into ferromagnetic rings by patterning an ellipse instead of a circular hole. We examine arrays of rings in two extreme limiting cases: symmetric rings with a concentric circular hole and asymmetric

* Electronic address: daniel.gopman@nist.gov.

rings with a concentric two–to–one aspect ratio elliptical hole. The 10 μm outer diameter ring size enables one to use magneto–optic indicator film (MOIF) microscopy and magnetometry to study the influence of lateral geometry on the domain formation and dynamics of these shaped elements. The transition fields and magnetization dynamics are strongly dependent on the symmetry of the inner patterning of the ring and the orientation of the applied magnetic field with respect to the asymmetric pattern.

The $Ni_{80}Fe_{20}$ (Permalloy) rings were defined using a lift–off process on a thermally oxidized Si substrate. Using e–beam lithography, we defined arrays of rings having a 10 μm outer diameter and either a 7 μm diameter circular hole or a 7 μm $\times$ 3.5 μm elliptical hole centered inside the outer circumference. Individual rings were separated by a distance of at least 20 μm in order to minimize magnetostatic interactions between rings.[12,13] Using electron beam evaporation, we deposited a 30 nm thick Permalloy film capped with a 3 nm protective Au layer.

All magneto-optical (MO) measurements were performed at room temperature. Visualization of domain structures was provided during the remagnetization process using the magneto-optical indicator film (MOIF) technique.[14,15] Real time MO imaging was made using a charge coupled device (CCD) camera capturing 13.6 frames per second while the magnetic field was linearly varied at a rate of 1.8 mT/s. When the sample is magnetized uniformly, the direction of the magnetization M can be determined by the orientation of the symmetry axis of the MO contrast formed by the components of the stray field at the edges of the Permalloy rings. A quantitative measure of magnetization is given by the averaged intensity of the MO signal:

$$\bar{I} = (I_D + I_B)/2, \quad (1)$$

where I_D and I_B are the maximal intensities on the dark and bright edges, respectively.[14,16] This value is determined by the angle of Faraday rotation of the polarized light, which is proportional to the perpendicular component of the stray field at the edge of the ring and, hence, to the in-plane magnetization projection along the symmetry axis averaged over the sample thickness.

Using the averaged intensity to represent magnetization, we evaluated the individual magnetization versus applied field curves of three–by–three arrays of rings with either a circular hole or an elliptical hole. Figure 1 demonstrates magnetization versus applied field hysteresis loops for a ring with an elliptical hole with field ($\mu_0 H$) along the long– and short–axes of the ellipse and for a ring with a circular hole. Magnetization configurations of the ring corresponding to an onion state, a vortex state and an anti–vortex state are depicted schematically on top of the hysteresis loops. The magnetization of the ring with an elliptical hole shows low remanence (less than 50%) and a narrow hysteresis loop with $\mu_0 H$ aligned along its short axis (blue diamonds and line). On the other hand, the magnetization with $\mu_0 H$ parallel to the long axis (green triangles/pentagons and line) shows nearly full remanence and a wider hysteresis loop, indicative of that being an easy magnetization direction. Taken together, these two findings are consistent with the expected shape anisotropy induced by the

elliptical hole. Furthermore, the narrowest regions at the top and bottom of these asymmetric rings can create a local energy minimum for head–to–head domain walls comprising the onion state, which also should enhance the magnetization at remanence.[5,11] Finally, we note that the magnetization of the ring with a circular hole (red squares and line) exhibits a larger coercive field than the ring with the elliptical hole for $\mu_0 H$ aligned along either symmetry axis of the ellipse. The circular hole samples also exhibit a wider field region of stability for the vortex state, suggesting that the broken planar symmetry makes the onion state more stable compared to the vortex state.

In order to interpret the magnetization curves shown in Fig. 1, we recorded a series of MOIF images at the points marked along decreasing branch (positive–to–negative applied magnetic field) of the three magnetization curves. Figure 2 presents an image for each of the magnetization states marked in these hysteresis curves. In the first column, we see the reversal of the ring with a concentric circular hole. At saturation, Figs. 2(a) and 2(e) show the largest magneto-optic (MO) contrast in regions where the rings are magnetized normal to the edges. At lower applied magnetic fields, the MO contrast pattern in the indicator film (Figs. 2(b) and 2(d)) is diminished, as the source of fringe fields in the rings is likely reduced to a region around the 180–degree domain walls of the onion state. More importantly, we demonstrate a nearly perfect in–plane flux–closure state in Fig. 2(c), as the light– and dark– contrast peaks near the top and bottom edges of the ring have disappeared with only small background contrast visible due to the moderate external field giving a small, non–zero net magnetization.The light contrast at the top of the interior hole reveals that the local magnetization has already reversed direction from “up” (as in Fig. 2(a)) to “down”.

We proceed to the middle column showing the easy–axis magnetization configurations generated by fields applied along the long (vertical) axis of the patterned elliptical hole. In Figs. 2(f) and 2(j), we observe magneto-optic contrast nearly reproducing the shape of the Permalloy ring. The fringe fields associated with the observed contrast pattern corresponds to magnetization pointing perpendicular to the edges of the inner and outer ring perimeters. In this case, the magnetization is nearly saturated along the vertical axis. At lower fields, the magnetization rotates away from the edges and the contrast emanating from the inner perimeter is no longer visible. Figures 2(g)–2(i) show a distribution of reversal fields for the individual rings, which could be due to variations in edge properties due to patterning, as well as to the intrinsic switching field distribution of each individual ring. We also notice an intermediate magnetization configuration in Figs. 2(g)–2(i), distinct from the uniform, onion and vortex states typically observed in microstructured rings. In particular, the alternating light and dark regions at nearly 45 ° from the ellipse long axis (along the diagonals) reveals a configuration in which the ring magnetization points outward along one diagonal and points inward toward the center along the opposite diagonal. This configuration resembles an anti–vortex configuration of the ring’s magnetization.

The origin of the anti–vortex can be understood by looking at Fig. 2(h), where we observe that while many of the rings exhibit dark contrast in the top–left and bottom–right quadrants, others show the opposite contrast orientation. It has been demonstrated previously that microstructured rings exhibit magnetization reversal by transitioning between onion states of

opposite magnetization orientation by the nearly simultaneous propagation and annihilation of domain walls.[6] The rings observed in this study possess an asymmetric lateral structure that could enable the independent reversal of the two wide, vertical magnetization segments. In that case, domain wall propagation along one vertical segment would lead to a metastable configuration in which the two vertical segments of the ring are magnetized anti–parallel, which would generate the anti–vortex pattern seen in our MOIF images.

Finally, we move to the right column showing the hard–axis magnetization states for the sample with an elliptical hole under fields applied along the short axis. Figures 2(k) and 2(o) exhibit uniform magnetization along the horizontal axis. In Fig. 2(l), we no longer can resolve the inner structure of the ring, suggesting that the fringe fields from the inner perimeter have been suppressed due to magnetization rotation. However, we do observe reversed contrast in the top and bottom horizontal segments of the ring, which reveals that magnetization reversal is initiated in these regions. In Figs. 2(m) and 2(n), we see that the MOIF contrast has circulated around the rings, as some of the rings have already started to reverse themselves by rotation. Finally, in Fig. 2(o), the magnetization is reversed, and again it is possible to observe fringe fields from the inner perimeter of the ring.

The magnetization configurations were also calculated using the Object Oriented Micromagnetic Framework (OOMMF) software code.[17] Typical material constants for Permalloy were chosen: saturation magnetization =860 kA/m, exchange stiffness=13 pJ/m, and magnetocrystalline anisotropy = 0 J/m^3. The discretization cell size was 5 nm × 5 nm × 5 nm. Applied fields in all simulations are oriented along the vertical axis, consistent with the experimental results shown in Figs. 2(a)– 2(j). Figures 3(a)– 3(c) show the progression of the magnetization in the ring with the circular hole from an initial vortex state at zero applied field, through an onion state at 50 mT applied field, and finally to the uniform state at 100 mT applied field. In these simulations, we find that at moderate negative fields, there is an onion–to–vortex transition, which agrees with the measured hysteresis loops and MOIF images shown in Fig. 1 and Figs. 2(l)–2(m), respectively. Micromagnetic configurations of the ring with the elliptical hole for fields applied along the long–axis reveal the absence of a vortex transition state, which is qualitatively in agreement with the hysteresis loops in Fig. 1 and the MOIF images in Fig. 2(f)– 2(j). However, the calculations were not able to produce the anti–vortex state seen in Figs. 2(g)– 2(i).

Figure 3(d) is the closest micromagnetic representation to our anti–vortex MOIF observations, but requires us to relax the ring at zero applied field from an initial anti–vortex state. This is additional confirmation that the non–uniform configuration that we observed is the outcome of inhomogeneity and stochasticity that are not incorporated in the present micromagnetics simulation, in which we assumed a defect–free system with no significant role of thermal effects. Additionally, our OOMMF simulations show that by applying a moderate field to this state along the ellipse long axis (10 mT), we can switch the “anti–vortex” into an onion state (Fig. 3(e)). Subsequently, with a sufficiently high applied field (100 mT), we are able to fully saturate the ring (Fig. 3(f)), which is qualitatively consistent with the behavior observed in the MOIF images in Fig. 2(g)– 2(i).

Lateral asymmetry in rings has been previously shown to significantly influence the reversal character, dictating in particular whether the ring magnetization evolves through a vortex state. Lateral ring thickness asymmetry speficially has been shown to enhance the probability of transitioning through a vortex state.[7,9] The present study has similarly explored the role of asymmetry by implementing an asymmetry in the lateral width of the rings through patterning of an elliptical hole with an aspect ratio of 2. We find that the magnetization rotation (Figs. 2(m)–2(n)) observed for fields applied along the ellipse short axis is consistent with reversal through vortex rotation. On the other hand, the magnetization configurations observed under fields applied along the long axis of the ellipse reveal the incoherent reversal of an onion state, which can be seen in both the two–step magnetization reversal in Fig. 1 as well as the “anti–vortex” configuration seen in the MOIF images presented in Figs. 2(g)–2(i).

We note that the preferred vortex or onion configuration induced by the ring width asymmetry is consistent with the effects of ring thickness asymmetry described earlier. However, this is the first time the incoherent reversal of the onion state has been demonstrated. Our micromagnetic simulations show that the “anti–vortex” configuration caused by incoherent onion reversal can be driven into a more standard, onion configuration with the application of an external field. This shows that the anti–vortex state is a transition state that transforms into an onion state under applied field, which is in agreement with our MOIF images.

In conclusion, we have presented MOIF magnetometry results on the role of internal geometry of microstructured Permalloy rings. By breaking the symmetry of the rings, we show that we can nearly eliminate the stability of the zero–flux vortex state found in an identical ring with a concentric circular hole. The remanent magnetization along the long–ellipse axis due to the added shape anisotropy was significantly enhanced, relative to magnetization along the short–axis and to the circular aperture ring. Furthermore, we saw the role of stochastic remagnetization processes through MOIF imaging of intermediate magnetization states along the long–ellipse axis that are anti–vortex–like. MOIF magnetometry measurements are obtained quickly, are non–destructive, and are well suited to understanding the magnetization reversal processes of materials on microscopic scales in transition from continuous films to the nanoscale.

Acknowledgments

We acknowledge June Lau for assistance with the micromagnetic simulations. J. C. and C. S. L. acknowledge support from the NSF Nanosystems Engineering Research Center for Translational Applications of Nanoscale Multiferroic Systems (TANMS) Cooperative Agreement Award (No. EEC–1160504).

References

1. Zhu J-G, Zheng Y, Prinz GA. Journal of Applied Physics. 2000; 87:6668.
2. Ross CA, Castao FJ, Jung W, Ng BG, Colin IA, Morecroft D. Journal of Physics D: Applied Physics. 2008; 41:113002.
3. Rapoport E, Montana D, Beach GSD. Lab Chip. 2012; 12:4433. [PubMed: 22955796]
4. Liang C-Y, Sepulveda AE, Hoff D, Keller SM, Carman GP. Journal of Applied Physics. 2015; 118:174101.

5. Rothman J, Kläui M, Lopez-Diaz L, Vaz CAF, Bleloch A, Bland JAC, Cui Z, Speaks R. Phys. Rev. Lett. 2001; 86:1098. [PubMed: 11178019]
6. Klaui M, Vaz CAF, Monchesky TL, Unguris J, Bauer E, Cherifi S, Heun S, Locatelli A, Heyderman LJ, Cui Z, et al. Journal of Magnetism and Magnetic Materials. 2004; 272276:1631.
7. Zhu FQ, Chern GW, Tchernyshyov O, Zhu XC, Zhu JG, Chien CL. Phys. Rev. Lett. 2006; 96:027205. [PubMed: 16486626]
8. Klaui M, Vaz CAF, Bland JAC, Heyderman LJ, David C, Sinnecker EHCP, Guimares AP. Journal of Applied Physics. 2004; 95:6639.
9. Singh DK, Yang T, Tuominen MT. Physica B: Condensed Matter. 2010; 405:4377. ISSN 0921-4526.
10. Richter, K.; Mawass, M.; Krone, A.; Krger, B.; Weigand, M.; Schtz, G.; Stoll, H.; Klaeui, M. 2015 IEEE Magnetics Conference (INTERMAG); 2015. p. 1ISSN 2150-4598
11. Richter K, Krone A, Mawass M-A, Krüger B, Weigand M, Stoll H, Schütz G, Kläui M. Phys. Rev. Applied. 2016; 5:024007.
12. Wang J, Adeyeye AO, Singh N. Applied Physics Letters. 2005; 87:262508.
13. Adeyeye AO, Goolaup S, Singh N, Wang CC, Gao XS, Ross CA, Jung W, Castao FJ. Journal of Physics D: Applied Physics. 2007; 40:6479.
14. Gornakov VS, Kabanov YP, Nikitenko VI, Tikhomirov OA, Shapiro AJ, Shull RD. Journal of Experimental and Theoretical Physics. 2004; 99:602.
15. Gornakov VS, Kabanov YP, Tikhomirov OA, Nikitenko VI, Urazhdin SV, Yang FY, Chien CL, Shapiro AJ, Shull RD. Physical Review B. 2006; 73:184428.
16. Kabanov Y, Zhukov A, Zhukova V, Gonzalez J. Applied Physics Letters. 2005; 87:142507.
17. Donahue, MJ.; Porter, DG. OOMMF: Object oriented micromagnetic framework. 2016. URL https://nanohub.org/resources/6539

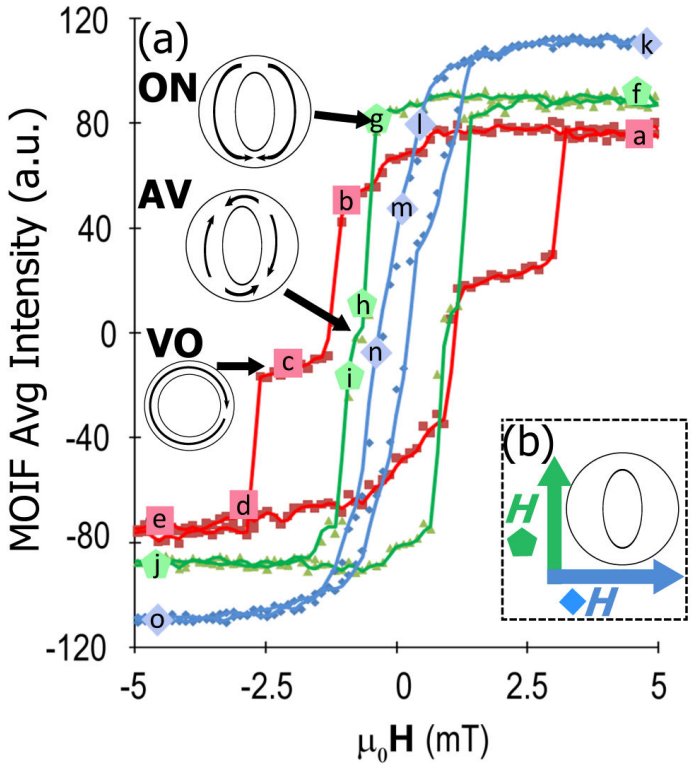

FIG. 1.

(a) MOIF magnetization versus applied external field for 10 μm rings with either a 7 μm concentric circular hole (red squares and solid line), an elliptical hole with field applied along the 7 μm long axis (green triangles/pentagons and solid line), or an elliptical hole with field applied along the 3.5 μm short axis (blue diamonds and solid line). Magnetization configurations of the ring corresponding to an onion state (ON), a vortex state (VO) and an anti–vortex state (AV) are shown schematically; (b) Orientation of applied field with respect to ellipse axes.

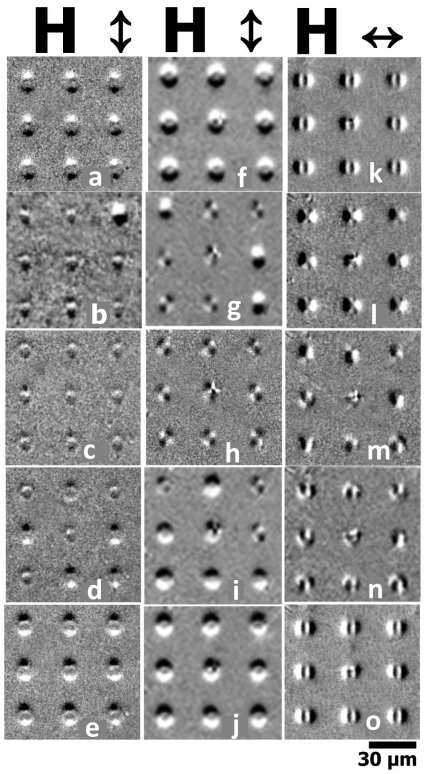

FIG. 2.

MOIF images during remagnetization: circular hole with vertical field (a–e) ; (f–j) elliptical hole with vertical field and (k–o) elliptical hole with horizontal field. Subfigures (a–o) correspond to fields along magnetization versus applied field data shown in Fig. 1.

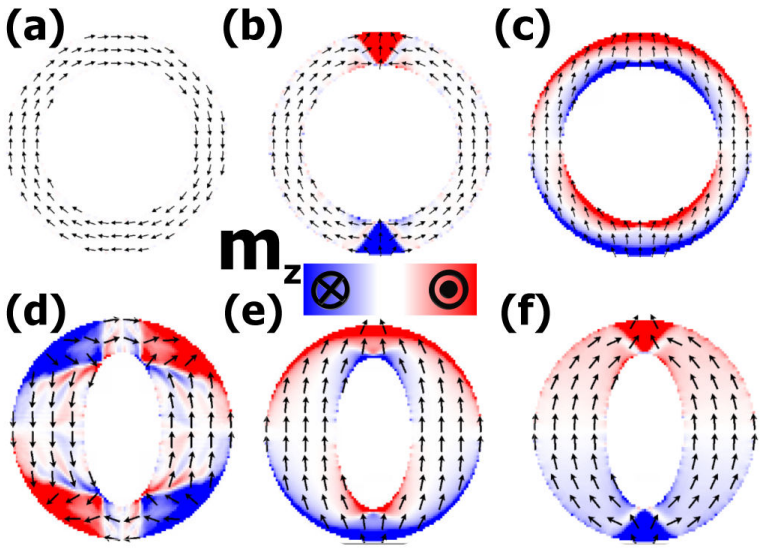

FIG. 3.

Micromagnetic simulation of 10 μm rings with a 7 μm concentric circular aperture (a) initialized in a vortex state, (b) under 50 mT vertical field after (a), and (c) under 100 mT vertical field after (b). Ring with an elliptical aperture (7 μm × 3.5 μm) (d) initialized in an anti–vortex state, (e) under 10 mT vertical field after (d), and (f) under 100 mT vertical field after (e). Arrows correspond to the planar magnetization and color coding reflects the out–of–plane magnetization component.